The dynamics and mixing of small spherical particles in a plane, free shear layer

Article *in* Physics of Fluids · May 1991

DOI: 10.1063/1.858049

2 authors:

Alfonso M Gañán-Calvo
Universidad de Sevilla
233 PUBLICATIONS **6,848** CITATIONS
SEE PROFILE

Juan Carlos Lasheras
University of California, San Diego
130 PUBLICATIONS **4,114** CITATIONS
SEE PROFILE

The dynamics and mixing of small spherical particles in a plane, free shear layer

Alfonso M. Gañán-Calvo and Juan C. Lasheras[a)]
Department of Mechanical Engineering, University of Southern California, Los Angeles, California 90089-1453

(Received 28 August 1990; accepted 22 January 1991)

The equation of motion of small rigid spheres settling under gravity in a two-dimensional inviscid flow given by the Stuart solution of the Euler equations is analyzed as a four-dimensional dynamical system. It is shown that depending on the values of the Stokes, Grashof, and a scaled Reynolds number, particles may either sediment or remain permanently suspended in the flow. When suspension occurs, the particle trajectories are shown to be attracted by a single period, quasiperiodic, or chaotic orbits. A consequence of the existence of a strange attractor (chaotic orbit) is that heavy particles can reach a stage of *fluidization* by which they remain indefinitely suspended in a layer of finite height located above the center of the Stuart vortices.

I. INTRODUCTION

The dynamics of particles in inhomogeneous and anisotropic turbulent flows is a problem highly relevant to a large variety of technological and geophysical applications. For example, in chemical reactors and combustors, the performance of the process is directly related to the spatial and temporal distribution of particles in mixing layers. Similarly, in natural flows, the transport of particulate pollutants in the atmosphere, the suspension of plankton in the oceans, or the transport of sediments in estuary and river beds also involves the dynamics and mixing of particles in inhomogeneous and anisotropic turbulent flows. Since in many of these industrial and geophysical flows, the concentration of particles is small enough for both their mutual interaction and their effect on the base fluid to be negligible, the dynamics and mixing of an isolated particle settling under gravity is the relevant problem to be studied.

Related studies of the gravitational settling of heavy particles in cellular and vortex flows have been reported by Stommel,[1] Tooby *et al.*,[2] Manton,[3] Maxey and Corrsin,[4] Nielsen,[5] Smith and Spiegel,[6] Maxey,[7] and McLaughlin,[8] among others. Stommel[1] first showed that small spherical particles may remain trapped indefinitely in a two-dimensional, incompressible, steady cellular flow. In experiments suggested by Stommel's results, Tooby *et al.*[2] found that in a vortex whose axis is perpendicular to the direction of gravity, heavy particles may follow closed trajectories. Manton[3] and Nielsen,[5] while analyzing a prototype flow represented by a Rankine vortex, found that particles with a settling velocity smaller than the maximum velocity of the vortex may remain indefinitely trapped in circular paths inside the vortex. Manton[3] then argued that, since turbulence is not completely incoherent, it could result in particles falling in a turbulent flow at a much slower rate than their terminal velocity, even in the absence of a mean updraft. Maxey[7] considered the combined effect of particle inertia and virtual mass on the gravitational settling of particles through an infinite, periodic Langmuir cellular flow field. He showed that, for arbitrary particle density, the inclusion of the effect of the inertia of both the particle and the fluid results in the existence of stable attractor sets for the dissipative, non-Hamiltonian system, whereby the particles collect along well-defined accumulation curves, with the individual particle trajectories merging into isolated asymptotic paths. In a recent related study, McLaughlin[8] has used perturbation methods to also show that the equation of motion of small rigid spheres in steady laminar flows takes the form of a dynamical system in which phase volume is not conserved. He considered a three-dimensional solution of the steady, incompressible Euler equation given by the Arnold–Beltrami–Childress (ABC) flows, and showed that particle inertia and virtual mass destroy Lagrangian turbulence with the particles captured by periodic or quasiperiodic orbits. When gravitational effects were included he found that in a narrow range of the ABC parameters, the particles could sediment chaotically.

Since the two-dimensional mixing layer is a classic example of an inhomogeneous, turbulent flow where a large-scale coherent motion dominates its evolution, we have selected it for our study. In a two-dimensional free shear layer, large-scale coherent vortical structures are known to exist at low (Winant and Browand),[9] moderate (Brown and Roshko),[10] and high Reynolds numbers (Dimotakis and Brown).[11] This coherent vortical structure is an essential feature in the development of a turbulent mixing layer, and it can be described as an endless redistribution of vorticity in space (Corcos and Sherman).[12] Recently Lázaro and Lasheras[13–15] have shown that the coherency of the base flow persists in particle laden flows, and that these large eddies play a dominant role in the dynamics and mixing of the particles in the turbulent mixing layer. To analyze the role of the coherent component of the turbulent motion on the dynamics of the particles, in this paper we will study the Lagrangian evolution of small, heavy spherical particles settling under gravity in a periodic free shear flow given by the Stuart's solution,[16] which is a steady, inviscid, incompressible solution of the two-dimensional Euler equation.

In our analysis of the long term evolution of the particle

a) Present address: Department of AMES, University of California, San Diego, La Jolla, California 92093-0411.

 0899-8213/91/051207-11$02.00

dynamics, we will use the generalized Basset–Boussinesq–Ossen solution of the unsteady Stokes motion of rigid spherical particles given by Tchen,[17] and recently modified by Manton,[3] Auton,[18] and Maxey and Riley.[19] Accounting for the inertia of the particle, its weight, and the viscous drag imparted by the flow, we will study the effect of particle size, turbulent intensity (or velocity amplitude), vorticity distribution, and gravity as a four parameter dynamical system. Following this approach, we will concentrate on the study of the mechanisms resulting in the long term suspension and transport of heavy particle settling in inhomogeneous and anisotropic turbulent flows. It will be shown that, depending on the above four parameters, long term suspension of heavy particles may occur. Furthermore, when suspension occurs, we will describe a new mechanism leading to the long time trapping of particles in vortical flows. We will show that the motion of the heavy particles may be attracted by periodic, quasiperiodic, or chaotic orbits. Physically, this long time fluidization stage is reached as a result of the combined effect of the convection by the mean flow, ejection from the unstable centers (inside the vortex cores), and gravitational settling. This new suspension mechanism differs significantly from the previously identified one whereby particles are trapped inside the vortex cores in close paths.

In Sec. II, we introduce the equation of the acceleration of the particle in the base flow selected for our study, and discuss the dynamical system formulation, the dimensionless governing parameters, and the numerical method used. In Sec. III, we present the numerical results and discuss the existence of several fluidization mechanisms. Special attention will be devoted to the study of the strange attractor defined by chaotic orbits. Finally, in Sec. IV, the main conclusions of this work are summarized.

II. FORMULATION OF THE PROBLEM

The flow field selected for our study is the steady, two-dimensional, inviscid solution of the Euler equations given by Stuart.[16]

The streamfunction $\Psi(x,y)$ is given by[16]

$$\Psi = \frac{\lambda U_0}{2\pi} \ln\left[\cosh\left(\frac{2\pi(y-y_0)}{\lambda}\right) - k_s \cos\left(\frac{2\pi(x-x_0)}{\lambda}\right)\right], \tag{1}$$

where λ is the distance between vortices, (x_0,y_0) are the spatial coordinates of the center of the reference vortex, and $\pm U_0$ is the free-stream velocity at either side of the mixing layer, $y = \mp \infty$, respectively. The value of the constant k_s determines the spatial distribution of vorticity: for $k_s = 1$, Eq. (1) reduces to a flow given by an array of point vortices separated by a distance λ, while for $k_s = 0$ it gives a uniform vorticity distribution solution characterized by the tanh streamwise velocity profile. In the present study, to model the coherent vortices of a two-dimensional turbulent shear layer, we have selected a periodic array of Stuart vortices with $k_s = 0.25$. The choice of the constant k_s is based on the experimental findings of Browand and Weidman.[20] Their results indicated that the time-averaged vorticity distribution measured in a turbulent mixing layer can be accurately reproduced by Stuart's solution with $k_s = 0.25$.

The two components u_f and v_f of the velocity field u_f are given by

$$u_f = -U_0 \times \frac{\sinh[2\pi(y-y_0)/\lambda]}{\cosh[2\pi(y-y_0)/\lambda] - k_s \cos[2\pi(x-x_0)/\lambda]} \tag{2}$$

and

$$v_f = U_0 \times \frac{k_s \sin[2\pi(x-x_0)/\lambda]}{\cosh[2\pi(y-y_0)/\lambda] - k_s \cos[2\pi(x-x_0)/\lambda]}. \tag{3}$$

The vorticity vector ω_f is

$$\omega_f = \left(\frac{2\pi U_0}{\lambda}\right) \frac{1-k_s^2}{\{\cosh[2\pi(y-y_0)/\lambda] - k_s \cos[2\pi(x-x_0)/\lambda]\}^2} \mathbf{k}, \tag{4}$$

where $\mathbf{k}$ is the unit vector in the spanwise z direction (see Fig. 1).

We consider the motion of a spherical, rigid particle of diameter d_p and density ρ_p in an unbounded fluid of density ρ_f and kinematic viscosity ν. Conservation of momentum for a small rigid sphere with diameter $d_p \ll \lambda$ is given by[17,19]

$$\begin{aligned}\frac{1}{6}\pi d_p^3(\rho_p + 0.5\rho_f)\frac{d\mathbf{u}_p}{dt} &= +\frac{1}{6}\pi d_p^3(\rho_p - \rho_f)\mathbf{g} + \frac{1}{4}\pi d_p^3 \rho_f \frac{D\mathbf{u}_f}{Dt} \\ &+ \frac{3}{2}(\pi\nu)^{1/2} d_p^2 \rho_f \int_0^t \frac{(D\mathbf{u}_f/D\tau - d\mathbf{u}_f/d\tau)}{\sqrt{t-\tau}} \\ &+ 3\pi\rho_f d_p \nu(\mathbf{u}_f - \mathbf{u}_p) f_1 + F_L,\end{aligned} \tag{5}$$

where subscripts p and f refer to the particle and fluid, respectively; $\mathbf{g}$ is the acceleration of gravity, considered normal to the plane of the mixing layer, and along the negative y axis; and the function f_1 is a correction for the viscous drag given by Cliff *et al.*:[21]

$$f_1 = 1 + 0.1315 \mathrm{Re}_p^{0.82 - 0.05 \log_{10} \mathrm{Re}_p}, \quad 0 < \mathrm{Re}_p < 20, \tag{6}$$

which can be extended to the range $20 < (\mathrm{Re}_p = |\mathbf{u}_r| d_p/\nu) < 200$ (with less than a 2% error), where $\mathbf{u}_r = \mathbf{u}_f - \mathbf{u}_p$ is the relative velocity between the particle and the fluid.

The terms appearing on the right-hand side of Eq. (5) represent, from left to right, the contribution to the acceleration of the particle of gravity, the nonuniformity of the far field stress tensor of the fluid, Basset history, drag, and lift forces.

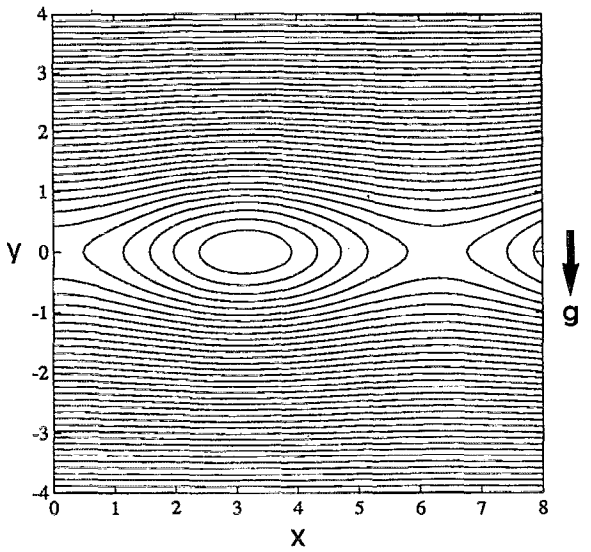

FIG. 1. Streamlines of the selected two-dimensional, steady flow given by Eq. (1) for $k_s = 0.25$. The physical coordinates are also shown in the figure. The symbol ⊙ stands for the outwards, spanwise, unit vector in the z direction.

Introducing scaling parameters,

$$T = \frac{dp^2}{18\epsilon\nu}; \quad L = \frac{\lambda}{2\pi}, \quad \text{where } \epsilon = \frac{\rho_f}{\rho_p + 0.5\rho_f}. \tag{7}$$

The dimensionless time (t^*), length (x^*), and velocities u_p^* and u_f^* are defined as

$$t^* = t/T; \quad x^* = x/L \tag{8}$$

and

$$u_p^* = \frac{2\pi}{\lambda}\frac{dp^2}{18\epsilon\nu}\mathbf{u}_p, \qquad u_f^* = \frac{2\pi}{\lambda}\frac{U_0\, dp^2}{18\epsilon\nu}\hat{\mathbf{u}}_f, \tag{9}$$

with $\hat{\mathbf{u}}_f$ given by

$$\hat{\mathbf{u}}_f = \{\hat{u}_f, \hat{v}_f\} = \left\{\frac{-\sinh y}{\cosh y - k_s \cos x}, \frac{k_s \sin x}{\cosh y - k_s \cos x}\right\}. \tag{10}$$

For heavy particles ($\epsilon \ll 1$) and for moderate values of A ($A < 30$), it can be shown that in the long term motion of the particle, the inertia, drag, and gravity terms are dominant and Eq. (5) reduces to the dimensionless form

$$\frac{d\mathbf{u}_p^*}{dt^*} = (A\hat{\mathbf{u}}_f - \mathbf{u}_p^*)f_1 + B\frac{\mathbf{g}}{|\mathbf{g}|}, \tag{11}$$

where

$$A = 2\pi U_0\, dp^2/\lambda(18\epsilon\nu) \tag{12}$$

is the inverse of the Stokes number, which is the ratio between the response time of the particle motion (T) and the characteristic time of change of the fluid velocity ($\lambda/2\pi U_0$); and

$$B = \frac{dp^2}{18\epsilon\nu}\frac{2\pi|g|}{\lambda}\frac{(\rho_p - \rho_f)}{(\rho_p + 0.5\rho_f)} \tag{13}$$

is a modified Grashof parameter.

The free-stream Reynolds number

$$\mathrm{Re}_p^* = \frac{U_0\, dp}{\nu}$$

is related to the instantaneous Reynold number Re_p by

$$\mathrm{Re}_p = (\mathrm{Re}_p^*/A)|A\hat{\mathbf{u}}_f - \mathbf{u}_p^*|; \tag{14}$$

the particle motion is then described by a four-dimensional, nonlinear autonomous dynamical system of the form

$$\dot{\mathbf{x}} = \mathbf{G}(\mathbf{x}), \quad \dot{x} \in \mathbf{R}^4, \quad \mathbf{G}: \mathbf{R}^4 \to \mathbf{R}^4,$$

whose components $\mathbf{x} = \{x_1, x_2, x_3, x_4\}$ and $\mathbf{G} = \{G_1, G_2, G_3, G_4\}$ are

$$\mathbf{x} = \begin{Bmatrix} x_p^* \\ y_p^* \\ u_p^* \\ v_p^* \end{Bmatrix}, \quad \mathbf{G} = \begin{Bmatrix} x_3 \\ x_4 \\ [A\hat{u}_f(x_1, x_2) - x_3]f_1 \\ [A\hat{v}_f(x_1, x_2) - x_4]f_1 - B \end{Bmatrix}. \tag{15}$$

Equations (10) and (15) with the initial conditions $\{x_p^*, y_p^*, u_p^*, v_p^*\}$ specified at $t^* = 0$, constitute a nonlinear, non-Hamiltonian dynamical system. Defining $\mathbf{J} = \partial\mathbf{G}/\partial\mathbf{x}$,

$$\mathrm{tr}\{\mathbf{J}\} = -2f_1 + u_p^*\frac{\partial f_1}{\partial u_p^*} + v_p^*\frac{\partial f_1}{\partial v_p^*} \neq 0. \tag{16}$$

Thus, system $\dot{\mathbf{x}} = \mathbf{G}$ does not preserve volume in the phase space.

We have investigated the use of several numerical integration algorithms to solve Eq. (11). Taking into account that we are studying the long time behavior of the system (15) and that the derivative functions are expensive to evaluate, we disregarded high precision algorithms such as the Bulirsch–Stoer extrapolation method or the Adams–Bashforth–Moulton predictor–corrector method. After comparison with a fourth-order Runge–Kutta algorithm, we selected a third-order multistep method such as

$$\mathbf{x}_{n+1} = \mathbf{x}_n + (\Delta t/2)(3\mathbf{G}_n - \mathbf{G}_{n-1}) \tag{17}$$

because we found it faster for a given accuracy. On the other hand, this algorithm performs a discretization of the continuous dynamical behavior into a mapping $\mathbf{R}^4 \to \mathbf{R}^4$. Thus, in order to retain the characteristics of our original system in the subsequent mapping and to avoid the creation of chaos resulting from the discretization procedure, as shown by Zufiria,[22] the step size Δt had to be small enough compared to the *period* of the original system, which is bounded by the period T_f of the flow motion. As a result of the fact that our system is strongly dissipative, for ratios $T_f/\Delta t$ larger than 10 we found that the mapping did not exhibit global changes. For the sake of accuracy, we chose $T_f/\Delta t > 50$.

In the following, using the analysis of nonlinear dynamical systems, we will focus our attention on the calculation of the long term evolution of the particle motion. In particular, our numerical study will be devoted to the following:

(i) In order to elucidate whether or not the long term suspension of particles can take place in our flow, we will

parametrically analyze via numerical simulation the geometry of the particle paths' attractors, their location, and their topology.

(ii) We will study the domains of attraction of the stable orbits to determine the spatial and temporal evolution of the particle concentration.

(iii) In order to gain knowledge into the existence of possible fluidization mechanisms, we will study the bifurcations of the solutions and the transition to chaos.

III. NUMERICAL RESULTS AND DISCUSSION

Before discussing the general results corresponding to our parametric study of the long term particle trajectory as a function of the three dimensionless governing parameters (A,B,Re*), and for the purpose of illustrating the nature of the different suspension regimes we found, we will begin presenting the dynamical behavior of heavy particles in a flow given by $U_0 = 7.5$ msec^{-1}, $\lambda = 10$ cm. This flow condition was selected in order to be able to qualitatively analyze the recent experimental studies of Lazaro and Lasheras.[15]

The bifurcation diagram giving the long term position (x_p,y_p) of a particle having zero vertical velocity ($v_p = 0$) is shown in Figs. 2(a) and 2(b) as a function of the particle diameter (dp). Note that corresponding to the selected flow conditions, particles of diameters smaller than 110 μm. are eventually collected along accumulation curves with each individual particle trajectory merging into a periodic asymptotic path represented by a one period limit cycle. For diameters greater than 110 μm, a first period doubling bifurcation occurs and the particles' paths were found to asymptotically converge into a two period orbit. For diameters larger than $\sim$117 μm the particle trajectories quickly reach a chaotic attractor.

A representative asymptotic particle trajectory corresponding to a one period limit cycle ($d_p = 109\,\mu$m) is shown in Fig. 3. Note in the figure that in this case, all particles that reached a long term suspension accumulated along a single path as the particles' trajectories asymptotically converged into a unique periodic orbit. Physically, this first mode of particle suspension results from the combined effect of the convection of the particles by the mean flow, the ejection from the unstable centers (vortex cores), and gravitational settling. It is interesting to note that this asymptotic path (Fig. 3) somewhat resembles the well-known bouncing ball trajectory. To further illustrate the nature of the attractor, the frequency power spectrum corresponding to the trajectories of particles of diameter 109 μm. is given in Fig. 4. Note that all the energy is accumulated into a single frequency representing a one period limit cycle.

As the particle diameter is increased, a period doubling bifurcation is found to occur for a diameter greater than 110 μm. A characteristic, asymptotic, two period, limit cycle trajectory resulting after the first period doubling bifurcation is shown in Fig. 5. Observe that, as was the case with a single period orbit, the structure of the attractor is such that all particles of the initial set reaching suspension accumulate along a single, two period orbit. The corresponding frequency power spectrum given in Fig. 6 shows the distinct appearance of a second peak located at the first subharmonic frequency, indicating the nature of the period doubling bifurcation. Notice also how the main peak has *shifted* toward lower values of the frequency, which corresponds to smaller values of the average horizontal velocity of the particle (or lower average vertical position of the trajectory).

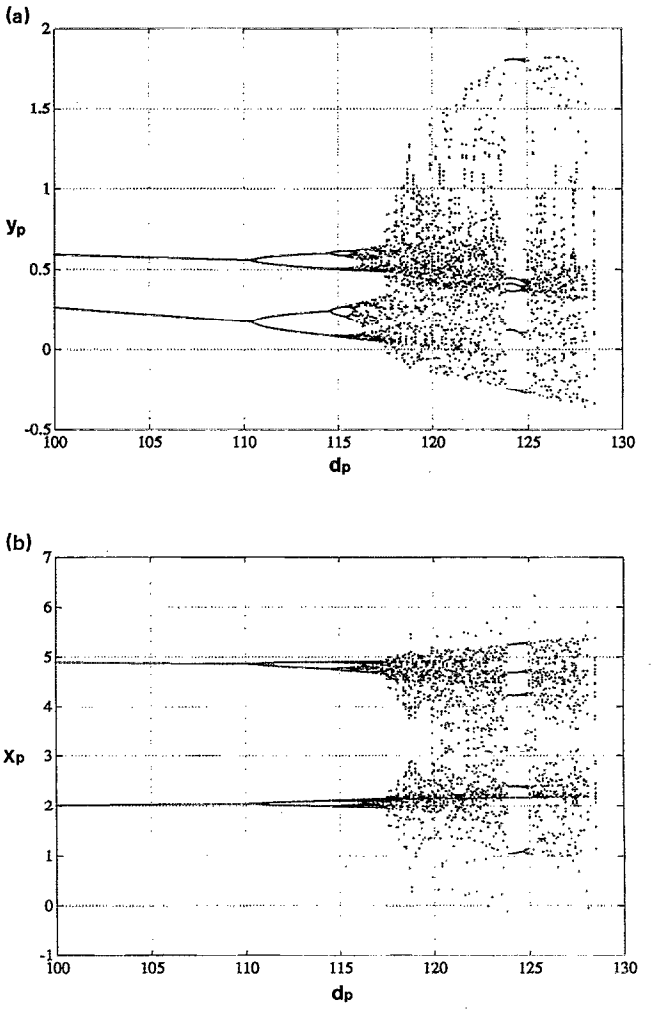

FIG. 2. Bifurcation diagram for a continuous range of particles of diameter d_p. (a) Vertical y positions and (b) horizontal x positions of the particle each time that its vertical velocity vanishes ($v_p = 0$).

As the diameter of the particle is further increased, a sudden bifurcation cascade leads to the particles' trajectories reaching a strange attractor characterized by chaotic orbits. In Fig. 7, the long term instantaneous positions of particles of diameter $d_p = 117\,\mu$m is shown. Observe that through the bifurcation cascade, the accumulation paths have now spread out over a well-defined layer located above the center of the Stuart's vortices. Physically, this transition to chaos in our dissipative, non-Hamiltonian, dynamical system represents the achievement of a long term *fluidization* stage whereby the particles remain permanently suspended in the flow in a layer of a given thickness. As opposed to the case of periodic orbits, the long term concentration of particles now loses the existence of singular regions along which the accumulation mechanism causes the concentration to become infinite. The corresponding projection in the $\{x,y\}$ plane

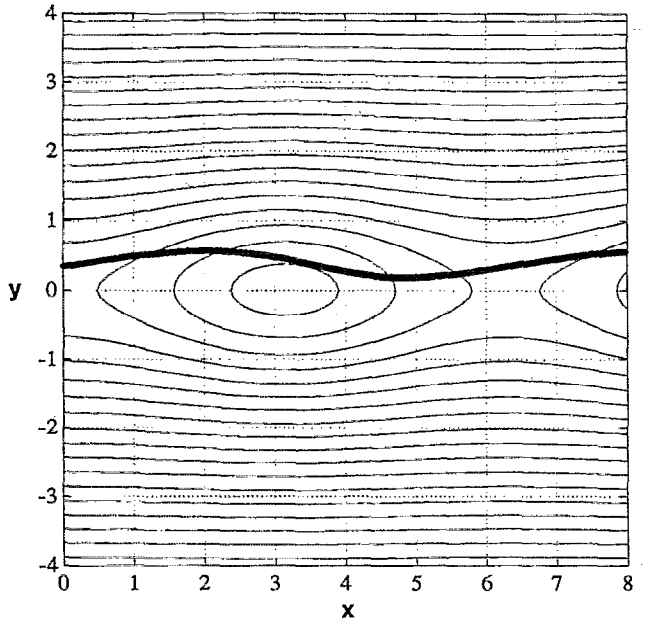

FIG. 3. One period, stable limit cycle corresponding to particles of diameter $d_p = 109\ \mu$m (see Fig. 2).

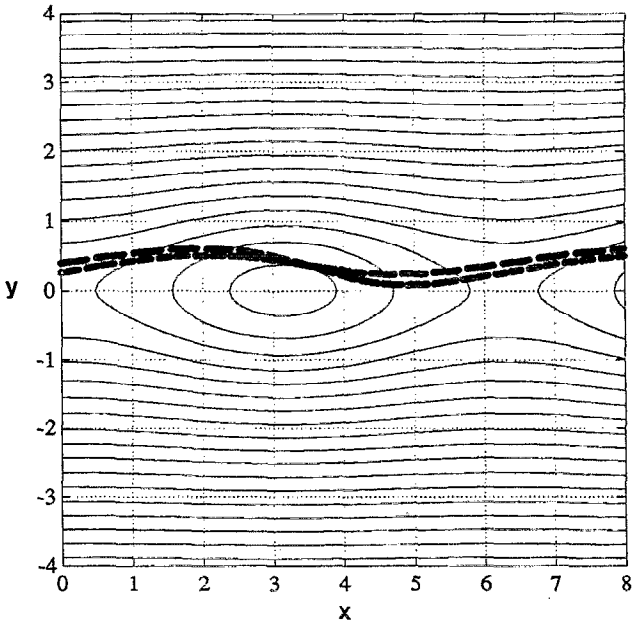

FIG. 5. Two period, stable limit cycle corresponding to particles of diameter $d_p = 114\ \mu$m.

(superimposed to the streamlines of the flow) of the three-dimensional Poincaré surface of sections of this chaotic orbit is given in Fig. 8. The frequency power spectrum of this quasiperiodic orbit is shown in Fig. 9. Observe that in addition to the coherent peaks, the spectrum now exhibits a well-characterized white noise level over a wide range of frequencies, indicating its chaotic character. Also observe a further shifting of the main peak toward lower values of the frequency.

For larger particle diameters, and through the bifurcation cascade, we found that the *fluidization* mechanism persists (Fig. 10). Furthermore, it was found that increasing particle diameters causes the widening of the *fluidization* region with the corresponding smoothening and lowering of the particle concentration values throughout (compare Figs. 7 and 10). In addition, as the *fluidization* region located above the Stuart's layer widens, the $\{x,y\}$ projection of the three-dimensional Poincaré surface of sections (Fig. 11) develops additional layers at higher vertical coordinates, and the frequency power spectra (Fig. 12) lose their coherency showing a broader frequency band of white noise now.

The sudden change in the chaotic attractor, which was found to occur for $d_p \sim 124\ \mu$m results from collisions between the chaotic attractor and a coexisting periodic orbit.[23] Grebogi *et al.*[24] were the first to observe this phenomenon. Similar *crises induced oscillations* have been also shown to occur in two- and three-dimensional maps and in three-

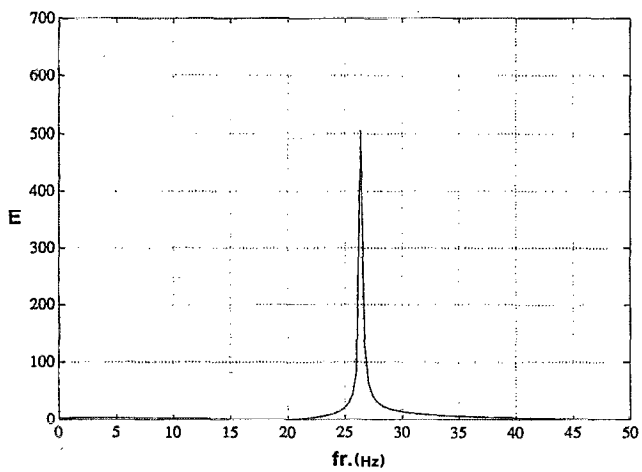

FIG. 4. Frequency power spectrum of the trajectories of particles of diameter $d_p = 109\ \mu$m. Observe the single peak representing the one period limit cycle.

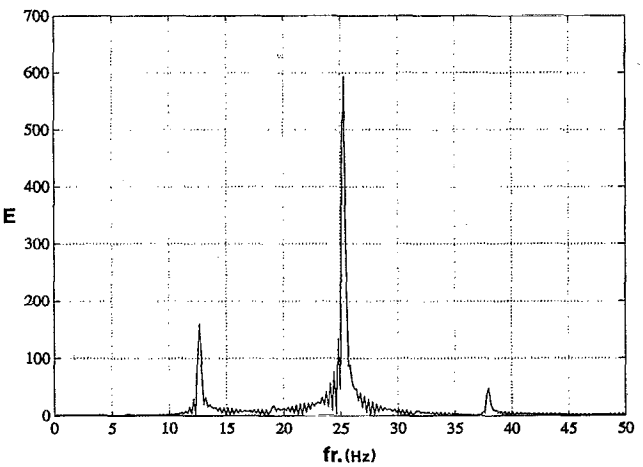

FIG. 6. Frequency power spectrum of the trajectories of particles of diameter $d_p = 114\ \mu$m. Observe the appearance of a second peak representing the subharmonic frequency of the trajectory, as well as a peak corresponding to the first harmonic frequency.

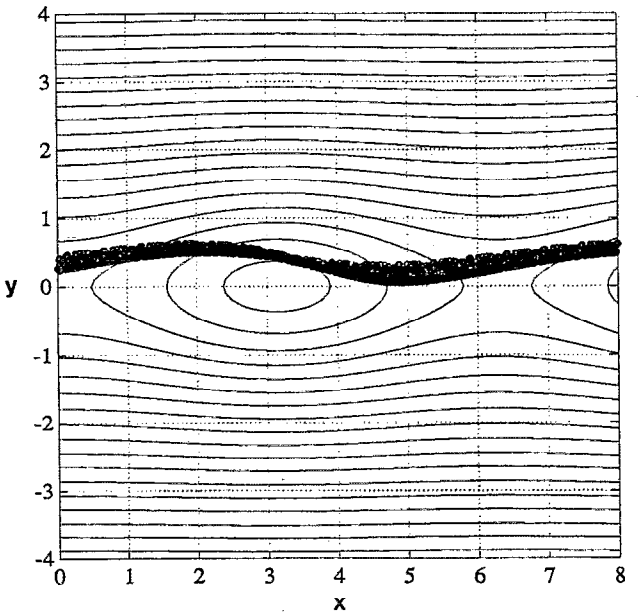

FIG. 7. Quasiperiodic, stable limit cycle corresponding to particles of $d_p = 117\,\mu$m.

dimensional flows. The presence of the above sudden change in the chaotic attractor with the appearance of a "crisis induced oscillation" of period three shows the chaotic nature of the trajectories after the bifurcation cascade.[25]

After having presented the case described above illustrating the existence of several long term suspension regimes, whereby heavy particles remain suspended indefinitely in a flow with zero mean vertical velocity, we will now discuss the result of a more general parametric study. In the

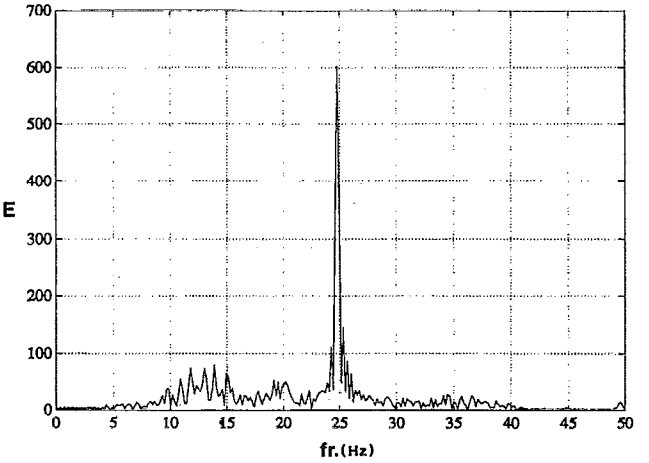

FIG. 9. Frequency power spectrum of the particle trajectory in Fig. 7.\

following, we will analyze the long term behavior of the particles' trajectories in the parameter space A, B, and Re_p^*/A. In particular, we will focus our attention on obtaining the parameter ranges for which the particles will either settle or will remain suspended in periodic, quasiperiodic, or chaotic orbits. Furthermore, for all of the different regimes when suspension occurs, we will discuss the geometry of the corresponding basin of attraction.

Hereafter, we will use the terms *stable* or *unstable* in a rather loose manner. We will call the system *stable* if the long term vertical position of at least one particle remains bounded (particle suspension). If all the trajectories are unbounded the system will be called *unstable* (particle settling).

We begin by presenting the dynamical behavior of system (15) in the parameter space $\{A,B,\mathrm{Re}_p^*/A\}$. The *stability* limits expressed as a function of the three governing dimen-

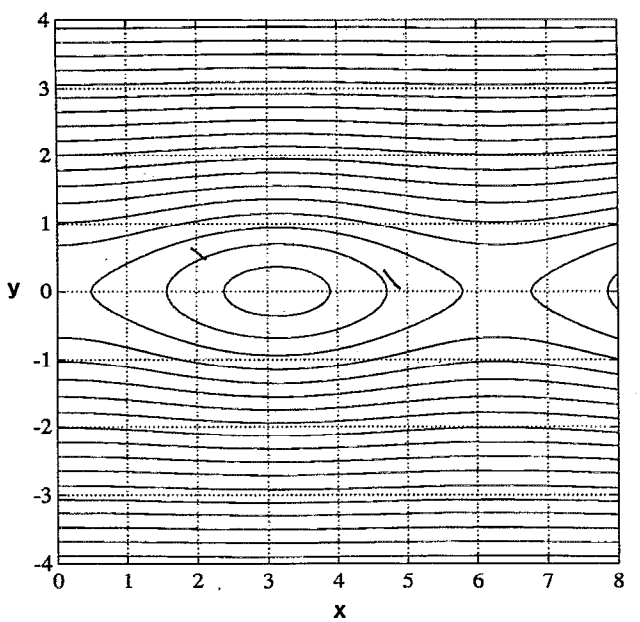

FIG. 8. Projection in the (x,y) plane of the Poincaré surface of sections for the trajectory given in Fig. 7, superposed to the flow streamlines.

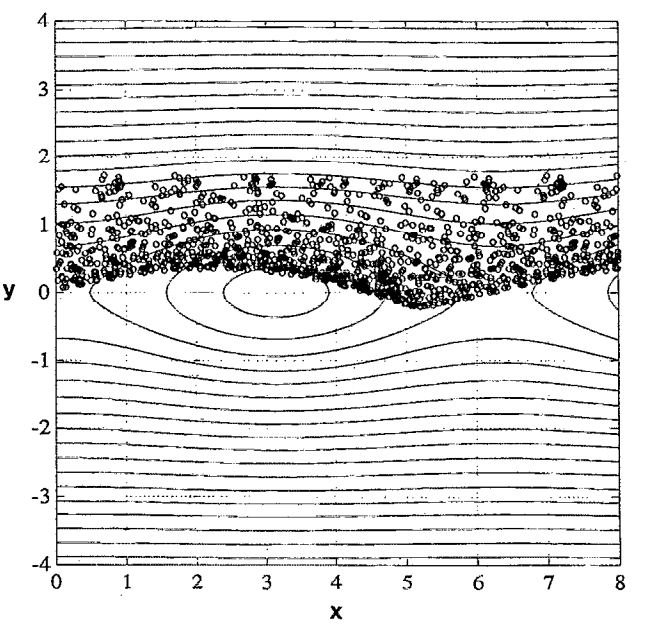

FIG. 10. Chaotic, stable orbit corresponding to particles of diameter $d_p = 123\,\mu$m.

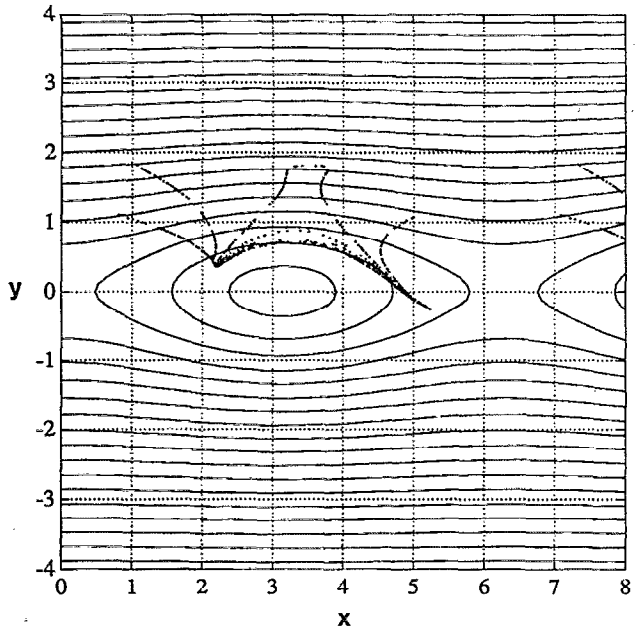

FIG. 11. Projection in the (x,y) plane of the Poincaré surface of sections for the trajectory given in Fig. 10, superposed on the flow streamlines.

sionless parameters are shown in Fig. 13. For each scaled Reynolds number (Re_p^*/A), the upper solid surface represents the range of Stokes (A) and Grashof (B) parameters for which the particle follows either a stable or an unstable path. In physical terms, this stability surface represents the boundary between the parameter region for which the long term particle evolution results either in a sedimentation or in a suspension. Above the solid surface in Fig. 13, all particles follow unstable trajectories, i.e., there are no particles in the set of initial conditions for which suspension can occur. Below this surface, a certain portion of the particles does not settle to $y = -\infty$, but follows a stable trajectory remaining indefinitely suspended in the flow. When suspension occurs,

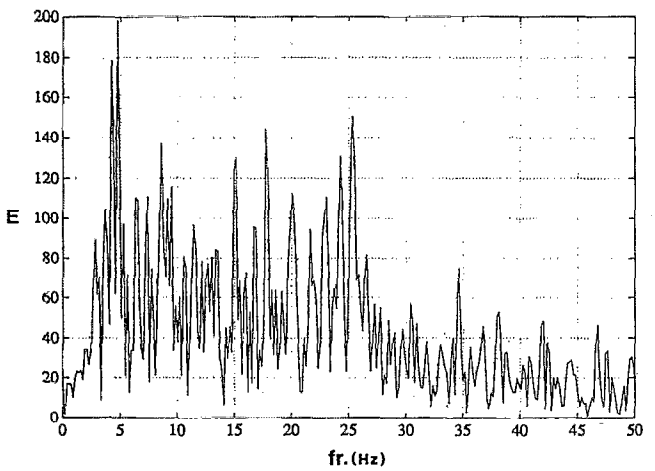

FIG. 12. Frequency power spectrum of the trajectories of particles of diameter $d_p = 123\ \mu$m. Observe the appearance of a broadband of white noise and the shifting of the main peak toward a lower frequency.

we found that the particles may follow periodic, quasiperiodic, or chaotic paths. The boundary representing the parameter range for which the particles follow a periodic path (one period limit cycle) or a quasiperiodic or chaotic one (two or more period limit cycles), i.e., first period doubling bifurcation, is also given in the figure (the lower surface represented by dotted lines). For a parameter combination below the lower surface, all suspended particles were found to remain in an asymptotic periodic path. Above this surface, by increasing the Grashof number B one finds a period doubling bifurcation and eventual transition to chaos.

These surfaces have been obtained by fitting with ninth-order polynomial functions a discrete set of (A,B) transition points calculated for several values of the scaled Reynolds number Re_p^*/A. The stability line and the location of the first period doubling bifurcation is shown in Figures 14(a)–14(d) for four representative values of Re_p^*/A. Note that as the Reynolds number increases, particle suspension may occur at larger values of both the Stokes and the Grashof parameters, and the parametric region of chaos widens.

A spectral analysis of the particle acceleration equation (10) reveals that a particle of a *given* diameter will respond with the same frequency spectra to a time periodic input with a period equal to, or larger than, its relaxation time. In the present case of particles settling under gravity in the Stuart layer, the gravitational parameter (B) is forcing the attractive limit cycles toward lower average horizontal velocity corresponding to larger input periods. On the other hand, when the particle remains suspended, its settling velocity must be of the order of the average vertical velocity that the particle experiences from the flow as it moves along the limit cycle. Since increasing the Grashof number (B) results in an increase in the settling velocity, the particle will follow lower and lower limit cycles until one of the following scenarios occurs.

(a) For small values of A ($A<1$), the period of the lower possible orbit is larger than the particle response time, and an increment in the Grashof parameter (B) causes the global settling of all the particles. In Figs. 14(a)–14(d), this case corresponds to the transition that results by increasing the parameter B for fixed values of A. To illustrate this, in Fig. 15(a) the lower possible stable orbit for a Stokes number $A = 0.56$ and $\mathrm{Re}_p^*/A = 17.9$ is shown. This case corresponds to a Grashof number $B = 0.0224$. Increasing B beyond this value results in sedimentation for all possible initial conditions of the particle as all the particles escape the attractor through the saddle point region.

(b) The period of the lower possible orbit is smaller than the particle response time (large A) and, in this case, the single period limit cycle bifurcates to a two period cycle having a longer period and a larger average vertical flow velocity. In this case, depending on the value of A, we found that increasing the Grashof number B leads to a transition F_0 settling either (i) from a multiple period orbit, (ii) from a quasiperiodic orbit, or (iii) from a chaotic trajectory. In the last case, by increasing B the period doubling lead to a bifurcation cascade by which the particle reaches quasiperiodic and chaotic orbits with a well-defined structure in the R^4 phase space. In Figs. 15(b) and 15(c) we show the lower

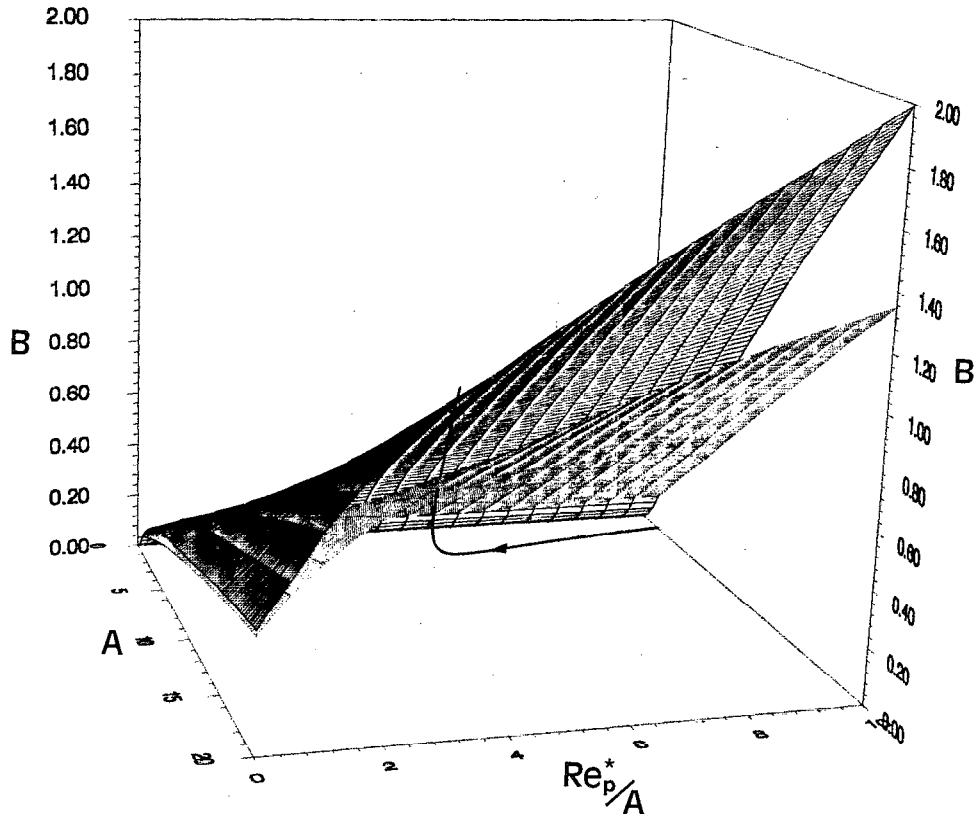

FIG. 13. Three-dimensional view of the surfaces delimiting the range of the three dimensionless parameters A, B, and Re_p^*/A for which the particle follows: (i) one period, stable limit cycles (space below the surface given by dotted lines); (ii) unstable—settling—trajectories (space above surface represented by solid lines); and (iii) two or more periods, stable limit cycles (space in between both surfaces).

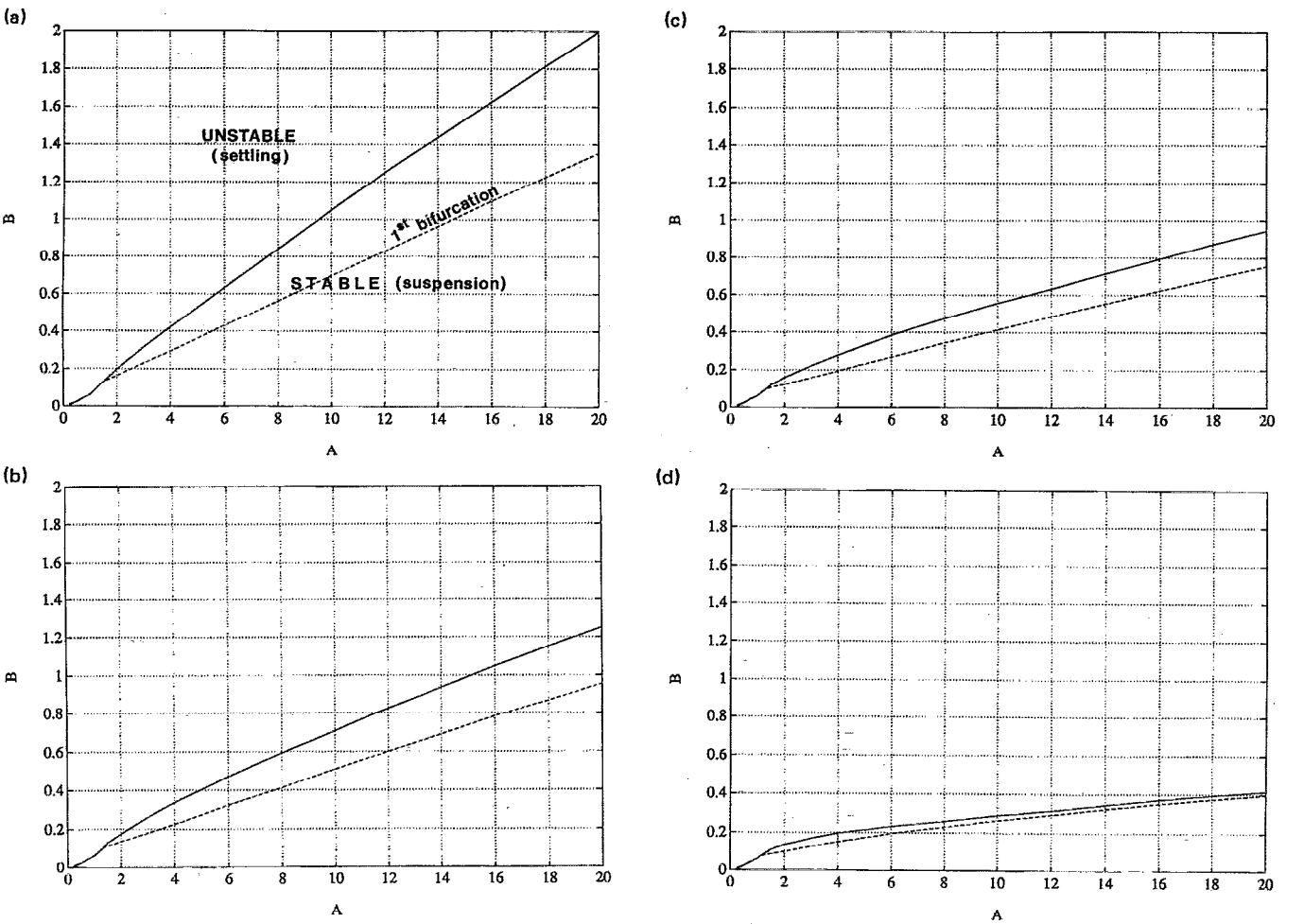

FIG. 14. Stability regions for (a) $Re_p^*/A = 10$; (b) $Re_p^*/A = 4$; (c) $Re_p^*/A = 2$; and (d) $Re_p^*/A = 0$.

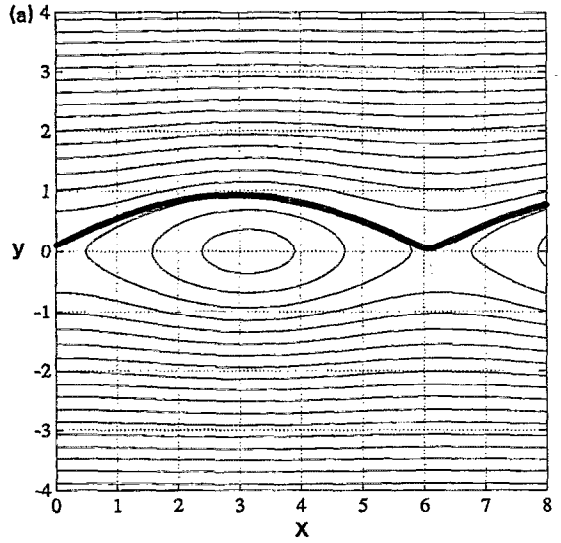

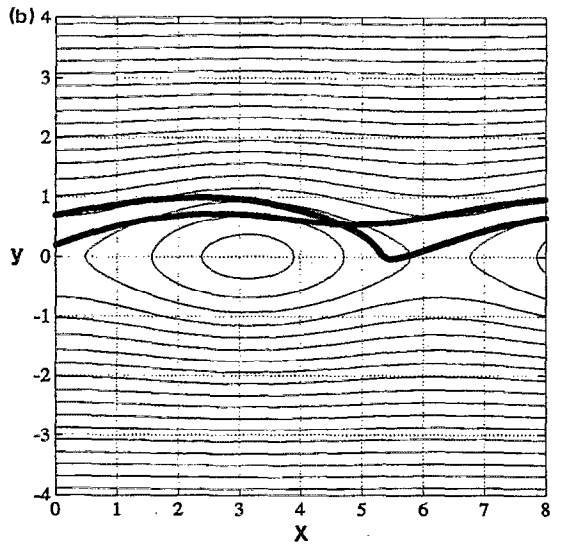

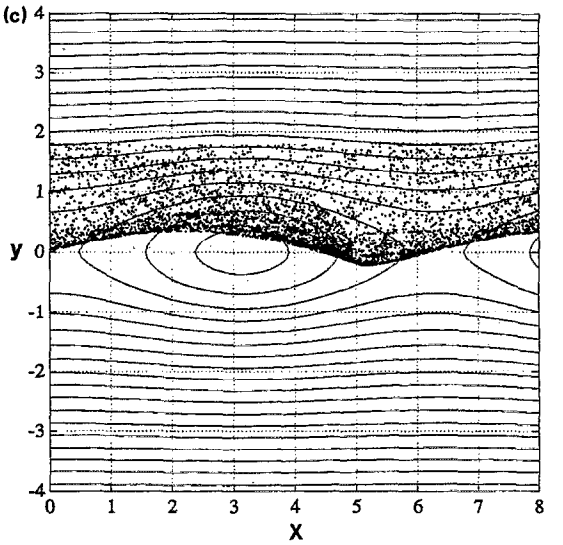

FIG. 15. (a) Lower possible one period, stable limit cycle for $A = 0.56$ and $\mathrm{Re}_p^*/A = 18$ (corresponding to a value of $B = 0.022$); (b) Lower possible two period, stable limit cycle for $A = 3.5$ and $\mathrm{Re}_p^*/A = 7.2$ ($B = 0.331$); and (c) Lower possible chaotic, stable orbit for $A = 20$ and $\mathrm{Re}_p^*/A = 3$ ($B = 1.1$). In the figure we have represented the instantaneous, long time positions of 4000 particles.

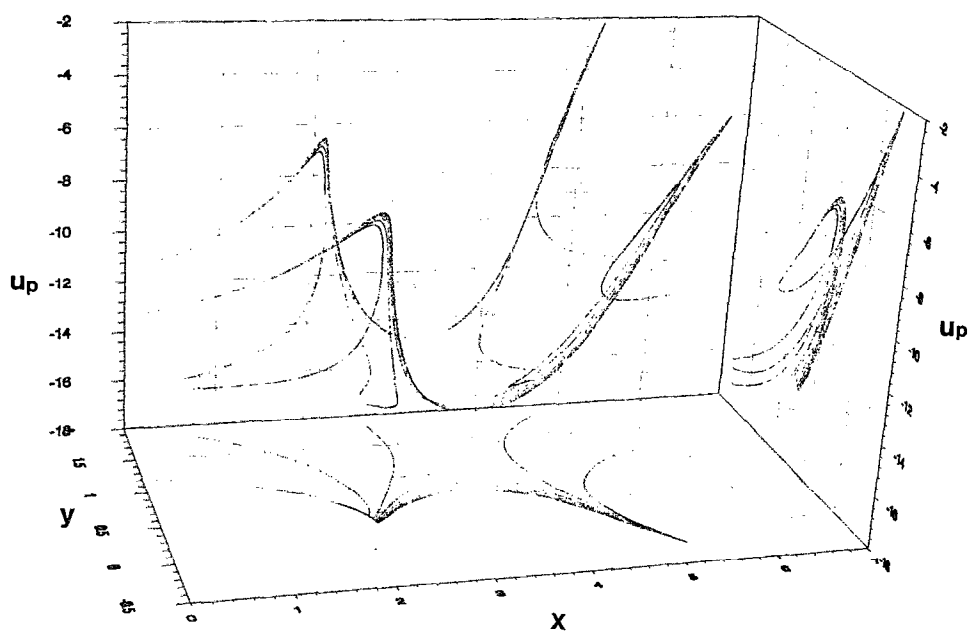

FIG. 16. Three-dimensional view of the Poincaré surface of section of the chaotic orbit in Fig. 5(c), and its projections on (x,y), (x,u_p), and (y,u_p) planes. The Poincaré surface of sections is computed by recording the position and the horizontal velocity of the particle each time that its vertical velocity $v_p = 0$. Observe the well-defined fractal geometry of the section.

stable, two period limit cycle for the case of a moderate Stokes number, and the lower chaotic cycle corresponding to a larger Stokes number, respectively. In both cases increasing B was found to lead to a transition to sedimentation. In Fig. 16, the structure of the Poincaré surface of sections formed by recording the particle coordinate each time that its vertical velocity becomes zero, is given. The flow conditions corresponding to this figure are the same as in Fig. 15(c). In this three-dimensional plot we show the well-defined fractal topology of the Poincaré surface of sections of our dynamical system in the chaotic regime.

In order to obtain information about the global, long term dynamics of particles in periodic flows, the study of the basin of attraction is another important issue. Given the probability distribution function of particles in the phase space $f(x,y,\dot{x},\dot{y};d_p)$ for $t=0$, the relative amount of particles that remain suspended in the shear layer is given by the integral of this function over the volume of the domain of attraction in the phase space

$$\alpha = \int_0^\infty \left(\int_{V_a(d_p)} f(x,y,\dot{x},\dot{x};d_p)\,dx\,dy\,d\dot{x}\,d\dot{y} \right) d(d_p), \qquad (18)$$

which can be approximated by

$$\alpha \simeq \sum_{i=1}^{N} \int_{V_a(d_{p_i})} f(x,y,\dot{x},\dot{x};d_{p_i})\,dx\,dy\,d\dot{x}\,d\dot{y}. \qquad (19)$$

This integration can be accomplished through the discretization of the continuum range of the particles' diameters d_p in families $\{d_{p_i}\}_{i=1,\ldots,N}$, by computing for each family the geometry of the basin of attraction $V_a(d_{p_i})$. A new, numerical, powerful tool is available for achieving the solution of this, otherwise intractable, global problem in R^4 and is called the *cell mapping method*.[26] The application of this method to our problem is currently in progress, and will be presented elsewhere. However, for a fixed pair of values (u_p, v_p) at $t=0$, the corresponding section of the domain of attraction in the physical space $\{x,y\}$ can be obtained by using a simple recording of the long term position of particles initially located in a grid. The sections of the basins of attraction for the orbits corresponding to Figs. 15(a), 15(b), and 15(c), computed for initial velocities of the particles equal to those of the flow, are represented in Figs. 17(a), 17(b), and 17(c), respectively. As the particles are chaotically suspended, it was found that the basin of attraction becomes a fractal object as its boundaries acquire more complicated shapes [Fig. 17(b)]. It is interesting to point out that our findings are similar to the results of Gwinn and Westervelt[27] obtained for a forced pendulum. At the onset of chaos,[27] they found that the basin of attraction loses its identity, which also occurs in our case, as shown in Fig. 17(c).

IV. CONCLUSIONS

We have presented an analysis of a four-dimensional dynamical system to investigate the gravitational settling of small heavy particles in a two-dimensional periodic flow given by the Stuart solution of the inviscid Euler equations.

For each scaled Reynolds number based on the velocity of the free stream (Re_p^*), we obtained the Stokes (A) and Grashof (B) parameter range for which the long term parti-

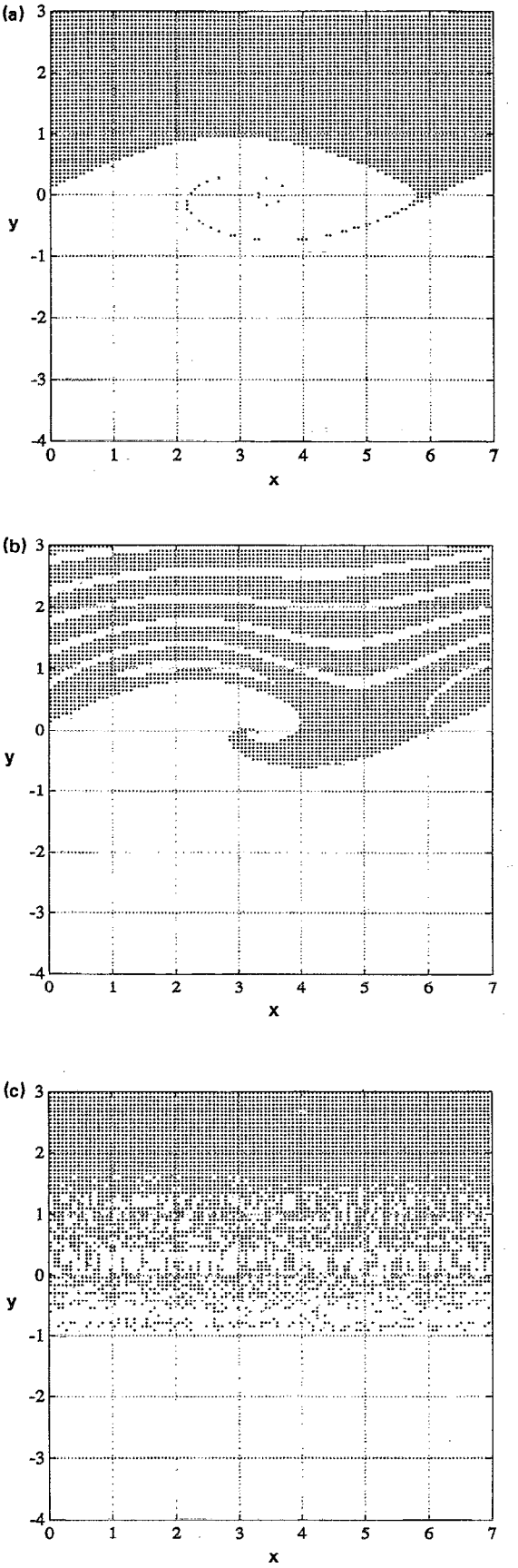

FIG. 17. Sections $[u_p = u_f(x,y)|_{t=0},\ v_p = v_f(x,y)|_{t=0}]$ of the domain of attraction in the phase space for the cases of (a) Fig. 15(a); (b) Fig. 15(b); and (c) Fig. 15(c).

cle motion resulted in either a sedimentation or in a suspension. In the range where suspension occured, we found that the particles were attracted by periodic, quasiperiodic, or chaotic orbits. For the case of periodic orbits, the particles were shown to accumulate along a unique, periodic path as all trajectories asymptotically converge into a single one. For the case of chaotic orbits, it was found that the particle accumulation paths spread out over a well-defined layer of a given height located above the centers of the Stuart vortices leading to a stage of long term fluidization. This fluidization of the particles resulted from the combined effect of the convection by the mean flow, ejection from the center of the vortices, and gravitational settling. Furthermore, this mechanism was shown to differ significantly from the one previously found by Stommel,[1] Maxey,[2] McLaughlin,[8] and others. In this new suspension regime, the particles, instead of remaining in closed trajectories, were now attracted by either periodic or chaotic orbits, always remaining above the center of the Stuart vortices.

ACKNOWLEDGMENTS

We would like to thank Dr. Pedro Zufiria, Dr. R. Guttalu, and Dr. H. Flashner for their comments and helpful suggestions.

A. M. G-C. was supported by a grant from the Secretaría de Estado de Universidades e Investigación from Spain (FPU-28687948). The partial support of a gift from United Technologies Corporation to J. C. L. is also acknowledged.

[1] H. Stommel, J. Mar. Res. **8**, 24 (1949).
[2] P. F. Tooby, G. L. Wick, and J. D. Isaacs, J. Geophys. Res. **82**, 2096 (1977).
[3] M. J. Manton, Boundary Layer Meteorol. **6**, 487 (1974).
[4] M. R. Maxey and S. Corrsin, J. Atmos. Sci. **43**, 1112 (1986).
[5] P. Nielsen, J. Geophys. Res. **89**, 616 (1984).
[6] L. A. Smith and E. A. Spiegel, in *Notes on Applied Physics* (Springer-Verlag, New York, 1984).
[7] M. R. Maxey, Phys. Fluids **30**, 1915 (1987).
[8] J. B. McLaughling, Phys. Fluids **31**, 2544 (1988).
[9] C. D. Winant and F. K. Browand, J. Fluid Mech. **63**, 237 (1974).
[10] G. L. Brown and A. Roshko, J. Fluid Mech. **64**, 775 (1974).
[11] P. E. Dimotakis and G. L. Brown, J. Fluid Mech. **78**, 535 (1976).
[12] G. M. Corcos and F. S. Sherman, J. Fluid Mech. **73**, 241 (1976).
[13] B. J. Lázaro and J. C. Lasheras, Phys. Fluids A **1**, 1035 (1989).
[14] B. J. Lázaro and J. C. Lasheras, submitted to J. Fluid Mech.
[15] B. J. Lázaro and J. C. Lasheras, submitted to J. Fluid Mech.
[16] J. T. Stuart, J. Fluid Mech. **29**, 417 (1967).
[17] C. M. Tchen, Ph.D. thesis, Delft University, Martinus Nijhoff, The Hague, 1947.
[18] T. R. Auton, J. Fluid Mech. **183**, 199 (1987).
[19] M. R. Maxey and J. J. Riley, Phys. Fluids **26**, 883 (1983).
[20] F. K. Browand and P. D. Weidman, J. Fluid Mech. **76**, 127 (1976).
[21] P. G. Saffman, J. Fluid Mech. **22**, 385 (1965).
[22] P. J. Zufiria, Ph.D. dissertation, University of Southern California, 1989.
[23] H. G. Schuster, *Deterministic Chaos* (Verlagsgesellshaft, Weinheim, 1989).
[24] C. Grebogi, E. Ott, and J. A. Yorke, Phys. Rev. Lett. **51**, 339 (1983).
[25] T. Y. Li and J. A. Yorke, Am. Math. Mon. **82**, 985 (1975).
[26] C. S. Hsu, *Cell-to-Cell Mapping: A Method of Global Analysis For Nonlinear Systems* (Springer-Verlag, New York, 1987).
[27] E. G. Gwinn and R. M. Westervelt, Phys. Rev. A **33**, 4143 (1986).